Calorimetric study of phase transitions for butyloxybenzylidene octylaniline in silica aerogels: Static and dynamic behavior

Zdravko Kutnjak and Carl W. Garland
School of Science and Center for Material Science and Engineering, Massachusetts Institute of Technology, Cambridge, Massachusetts 02139
(Received 1 August 1996)

The quenched randomness and surface effects associated with high-porosity aerogels can have substantial effects on the phase transitions in thermotropic liquid crystals. A high-resolution ac calorimetry and relaxation calorimetry investigation has been carried out on butyloxybenzylidene octylaniline (4O.8) in two silica aerogels with mass densities $\rho=0.08$ and 0.17 g cm^{-3}. Bulk 4O.8 exhibits weakly first-order nematic-isotropic, second-order nematic–smectic-*A*, and strongly first-order smectic–*A*–crystal-*B* transitions. In both aerogels, all of these transitions become continuous; 4O.8 in the $\rho=0.17$ aerogel exhibits substantial dynamical behavior. Measurements over a range of frequencies from 2.23 to 31.25 mHz allow one to obtain the static specific-heat capacities. [S1063-651X(97)03101-2]

PACS number(s): 64.70.Md, 61.30.−v, 65.20.+w, 82.70.−y

I. INTRODUCTION

The behavior near phase transitions of fluid systems in porous media is an active field of current research. During the past few years, a variety of investigations has been carried out using thermotropic liquid crystals as the fluid component [1]. These studies have included calorimetric measurements on liquid crystals in a variety of porous glasses [2,3], millipore filters [4], and silica aerogels [5,6]. The most detailed liquid-crystal plus aerogel study is for octylcyanobiphenyl (8CB) in a series of four aerogels of different porosities [5]. 8CB is a polar molecule that forms a partial bilayer smectic-A_d phase. The phase sequence on cooling is isotropic (I), nematic (N), smectic-A_d (Sm-A_d) and crystalline (K). Due to coupling between smectic and nematic order parameters, the second-order N–Sm-A_d transition lies in a crossover region between XY and tricritical behavior and the effective critical exponent for bulk 8CB is $\alpha=0.3$ [5]. In aerogels, both the N-I and the N–Sm-A_d heat-capacity peaks are shifted to lower temperatures and significantly rounded. These effects are most dramatic for the N–Sm-A_d C_p peak, which is greatly reduced in magnitude relative to the bulk peak.

The present work involves a detailed calorimetric study of the nonpolar liquid crystal *N*-(4-*n*-butyloxybenzylidene)-4′-*n*-octylaniline (4O.8)

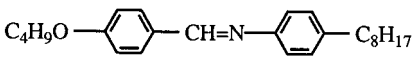

in two aerogels with mass density $\rho=0.08$ and 0.17 g cm^{-3}. These aerogels are the same as the two lowest-density (highest-porosity) gels used in the 8CB-aerogel study [5]. Bulk 4O.8 exhibits N-I, N–Sm-A_m, Sm-A_m–Cr-B, and Cr-B–K transitions, where Sm-A_m is a monolayer smectic with layer thickness d equal to the molecular length l, Cr-B is a plastic crystal-B phase, and K is the rigid crystal form stable at room temperature. The notation Sm-A_m is used to distinguish nonpolar monolayer smectic liquid crystals from polar liquid crystals that can exhibit both monolayer ($d\simeq l$) Sm-A_1 and bilayer ($d\simeq 2l$) Sm-A_2 phases. For convenience the subscript m will be suppressed in the subsequent text and Sm-A will be used for the 4O.8 monolayer smectic liquid crystal. The heat capacity associated with transitions in bulk 4O.8 has been well characterized by high-resolution ac calorimetry [7,8]. The N-I transition is typical of that seen in all liquid crystals: first order with substantial pretransitional wings. The second-order N–Sm-A transition has an effective critical exponent $\alpha=0.13$ [8] since the nematic range is larger than in 8CB and the smectic-nematic coupling is weaker. Furthermore, the integrated area δH_{NA} of the N–Sm-A heat-capacity peak is large (almost three times that for 8CB). The Sm-A–Cr-B transition is strongly first order with quite small pretransitional wings [7].

The goal of the investigation was to characterize the effect of quenched disorder associated with high-porosity aerogels on the phase transitions of a smectic liquid crystal that differs in several ways from 8CB. 4O.8 is a nonpolar molecule that contains an alkoyx oxygen and an imino nitrogen, both of which can hydrogen bond to hydroxyl groups on the silica surface, whereas 8CB does not have hydrogen bonding capability. Of special interest in the case of 4O.8-aerogel systems is the Sm-A–Cr-B freezing-melting transition, which has not been observed previously in liquid-crystal–aerogel systems, and the N–Sm-A transition, where the smectic-A structure and bulk C_p critical exponent differ significantly from those for 8CB. The large magnitude δH_{NA} of the N–Sm-A C_p peak is also an experimental advantage since aerogels greatly suppressed this feature in 8CB. Data obtained with an ac calorimeter over a substantial frequency range revealed an intrinsic dynamics, especially for 4O.8 in the $\rho=0.17$ aerogel. Thus the heat capacity is a complex frequency-dependent quantity with real and imaginary [Re$C_p(\omega,T)$ and Im$C_p(\omega,T)$] components.

The experimental procedures are briefly summarized in Sec. II. The results and an analysis of the dynamics for 4O.8 in the $\rho=0.17$ aerogel are given in Sec. III. A discussion of the static C_p behavior for 4O.8-aerogel systems and a comparison with analogous features in 8CB-aerogel systems are

given in Sec. IV, which also includes a discussion of the dynamic aspects of our data.

II. EXPERIMENTAL PROCEDURES

The two aerogels used in this work were from the same batches as those used previously for the study of 8CB-aerogel systems [5]. These aerogels were prepared by base-catalyzed polymerization of tetramethylorthosilicate and have a fractal network structure. For the aerogel with density $\rho = 0.08$ g cm^{-3}, the average pore chord L is 700 ± 100 Å and the volume fraction ϕ_p of pores is 0.945. For the $\rho = 0.17$ g cm^{-3} aerogel, L is 430 ± 65 Å and ϕ_p is 0.90. Further details about these aerogels are given in Ref. [5].

The empty aerogel pieces were thin slabs (0.65 mm thick) with plane-parallel faces and cross-sectional areas of ~ 0.6 cm^2, which were vacuum dried prior to filling. Filled 4O.8-aerogel samples were prepared in vacuum by heating 4O.8 into the isotropic phase and allowing the aerogel slab to fill slowly by capillary action. This procedure leaves the aerogel structure intact and does not create any empty regions [5,9]. After the filling was complete, the surface of the sample was dried with filter paper to remove excess bulk liquid crystal that might be present and the sample was weighed to determine the mass of 4O.8 in the gel (typically 30–50 mg).

The filled samples were then placed in a silver cell with attached heater and thermistor thermometer. The handling procedure was crucial since it was necessary to avoid having the 4O.8 freeze into the rigid crystal K phase. Preliminary runs established that these highly porous aerogel networks were severely damaged by the strains associated with going into the K phase (which occurs for bulk 4O.8 at 311 K [7]), and this has been confirmed by a detailed study of such damage effects in both 8S5-aerogel and 4O.8-aerogel systems [6]. Extensive data involving cycling through the Sm-A–Cr-B transition showed that freezing into the Cr-B phase had no damaging effect that influenced the C_p behavior. This is not surprising in view of the fact that Cr-B is an extremely soft plastic crystal phase. It should be noted that extensive data could be obtained on 4O.8-aerogel samples down to ~ 300 K with no indications of freezing into the K phase over moderate (several hours) time periods below the bulk freezing temperature of 311 K.

The transition temperatures were very stable (shifting down only 30 mK over 60 d of data acquisition) for samples in cells having a cold-weld indium seal. Samples in cells with the silver foil cover mechanically crimped onto a flange on the body of the cell showed larger shifts in transition temperatures (-14 mK/d), but the C_p behavior in transition regions was reproducible for different runs on several separate samples.

The high-resolution calorimeters used in this investigation have been described elsewhere [10]. It is possible to operate in two distinct modes. One is a conventional ac calorimetry mode, modified to allow one to measure C_p at many frequencies at a constant temperature and then step the temperature slightly and repeat the process. The second mode is a ramped relaxation (or nonadiabatic scanning) technique that uses dc heating and is capable of determining enthalpy changes including latent heats at first-order transitions. Details of this second mode of operation are given in Ref. [10]. Since relaxation runs were made over a wide temperature range of ~ 40 K, it was necessary to use ramp rates dT/dt of about ± 0.25 K/min, which resulted in somewhat noisy $C_p(T)$ data but allowed a run to be completed in 3 weeks.

Very extensive sets of data were obtained with the ac calorimetry mode. The standard operating frequency ω_0 used in the past for the oscillating heat input $P_{\rm ac}\exp(i\omega t)$ and the resulting $T_{\rm ac}$ oscillations was $\omega_0 = 0.1963$ s^{-1}, corresponding to a 32-s period for the $T_{\rm ac}$ signal or a frequency $\omega_0/2\pi$ of 31.25 mHz. In almost all past cases, this frequency is low enough to yield static ($\omega \to 0$) heat-capacity values. However, relaxing complex heat capacities $C^*(\omega,T)$ with a frequency dependence in this low-frequency range have been observed for a smectic-hexatic transition [10]. A similar situation has been observed for the two 4O.8-aerogel samples. In this case, the heat capacity of the sample cell has real and imaginary components: $C^*(\omega,T) = C'(\omega,T) - iC''(\omega,T)$. The equations for obtaining $C'(\omega,T)$ and $C''(\omega,T)$ from the observed amplitude $|T_{\rm ac}|$ and phase shift ϕ of the ac temperature oscillations are

$$C'(\omega) = \frac{|P_{\rm ac}|}{\omega |T_{\rm ac}|}\cos\phi, \tag{1}$$

$$C''(\omega) = \frac{|P_{\rm ac}|}{\omega |T_{\rm ac}|}\sin\phi - \frac{1}{\omega R}, \tag{2}$$

where $\Phi \equiv \phi - \pi/2$ is the phase shift of $T_{\rm ac}$ with respect to $P_{\rm ac}$. The quantity R is the thermal resistance of the thermal link (support wires and air) between the sample and the temperature-controlled thermal bath. The term $1/\omega R$ in Eq. (2) takes into account the effect of the nonadiabatic conditions (heat exchange with the surroundings). The value of R was determined in two independent ways: from relaxation data (see Ref. [10] for details) and from an analysis of very-low-frequency ac data taken at temperatures far from transition regions. The values of R from these two methods agreed well. It should be noted that Eq. (2) describes a one-phase system with both heat exchange and an intrinsic imaginary component of the heat capacity. When two-phase coexistence occurs at a first-order transition there is a distortion of the $T_{\rm ac}$ wave form that results in a characteristic anomalous peak in ϕ not described by Eq. (2). Examples of this familiar coexistence anomaly in ϕ are given in Refs. [5], [11] and [12].

The real and imaginary specific-heat capacities of 4O.8 in an aerogel are given by

$$\mathrm{Re}C_p(\omega,T) = [C'(\omega,T) - C(\text{cell} + \text{empty aerogel})]/m, \tag{3}$$

$$\mathrm{Im}C_p(\omega,T) = C''(\omega,T)/m, \tag{4}$$

where m is the mass of 4O.8 in grams and C (cell plus empty aerogel) is a real frequency-independent quantity determined at ω_0. Two types of ac data acquisition were used. In one type, ω was held constant and the temperature was scanned at a typical rate of 200 mK/h. Most of these runs were done on cooling, but some carried out on heating were in good agreement with cooling runs. For the $\rho = 0.08$ aerogel sample T scans were made at $2\omega_0$ and $\omega_0/5$. For the $\rho = 0.17$ aerogel samples T scans were made at ω_0, $\omega_0/9$, $\omega_0/22$, and $\omega_0/35$.

TABLE I. Latent heats ΔH and integrated enthalpies δH, in units of J mol^{-1}, for phase transitions in bulk 4O.8 and 4O.8 in silica aerogels of density ρ. Note that the molecular weight of 4O.8 is 365.56 g mol^{-1}. Also given are the shifts in the C_p peak positions with respect to those in bulk 4O.8: $\Delta T_c = T_c$(aerogel) $- T_c$(bulk). For each transition, two ΔT_c (K) values are cited; the value in parentheses pertains to a small sharp spike in C_p on the high-temperature side of the principal aerogel C_p peak.

Quantity	Bulk	$\rho = 0.08$ aerogel	$\rho = 0.17$ aerogel
ΔH_{NI}	1230	~ 0	~ 0
δH_{NI}	1570	2200 ± 150	2000 ± 150
δH_{NA}	800	620 ± 30	560 ± 30
ΔH_{AB}	1850	~ 0	~ 0
δH_{AB}	250	1670 ± 100	1450 ± 100
ΔT_{NI}		-4.9 (-4.4)	-5.4 (-4.5)
ΔT_{NA}		-4.0 (-3.0)	-4.5 (-2.8?)
ΔT_{AB}		-2.9 (-1.4)	-3.6 (-1.2)

The second type of run involved holding T constant (to within ± 0.1 mK) and taking data at 12 frequencies in the range $\omega_0 - \omega_0/14$ (31.25–2.23 mHz) and then stepping T slowly such that the scan rate was -20 mK/h in the vicinity of phase transitions.

III. RESULTS AND ANALYSIS

Before studying the 4O.8-aerogel samples, relaxation data were obtained on bulk 4O.8. Cells containing bulk liquid crystal were prepared in the same manner as used previously [10]. A relaxation run carried out from 357 K down to 310 K yielded the transition temperatures and enthalpies. The bulk transition temperatures were $T_{NI} = 353.10$ K, $T_{NA} = 337.10$ K, and $T_{AB} = 322.40$ K, in good agreement with previously published values [7]. The transition enthalpy values are listed in Table I, where ΔH represents the latent heat associated with a first-order transition with two-phase coexistence and δH is the integrated area of second-order peaks or pretransitional wings. $\delta H = \int \Delta C_p dT$, where ΔC_p is the excess heat capacity associated with a transition (i.e., the area above a smooth background curve, as described in Ref. [5]). It was difficult to separate the total N-I transition enthalpy of 2800 ± 150 J mol^{-1} into latent heat and pretransitional components. We estimate from the wings of the relaxation run that $\delta H_{NI} = 1400 - 1800$ J mol^{-1}. The value of 1570 J mol^{-1} for δH_{NI} given in Table I is taken from previous ac calorimetry data [7]. The values of δH_{NA} and δH_{AB} determined here agree well with the values 770 and 210 J mol^{-1} reported previously [7].

In addition to the relaxation run on bulk 4O.8, we also measured C_p in the vicinity of the second-order N–Sm-A transition with ac calorimetry at $2\omega_0$ (T scan rate 50 mK/h) and $\omega_0/5$ (T scan rate 30 mK/h). C_p data at both frequencies on heating and on cooling runs all agreed well with each other, indicating that dynamics does not play a significant role for bulk 4O.8 at these frequencies and the data can be considered to be static specific-heat capacities. These ac data could be fit very well with the usual power-law form including corrections-to-scaling terms

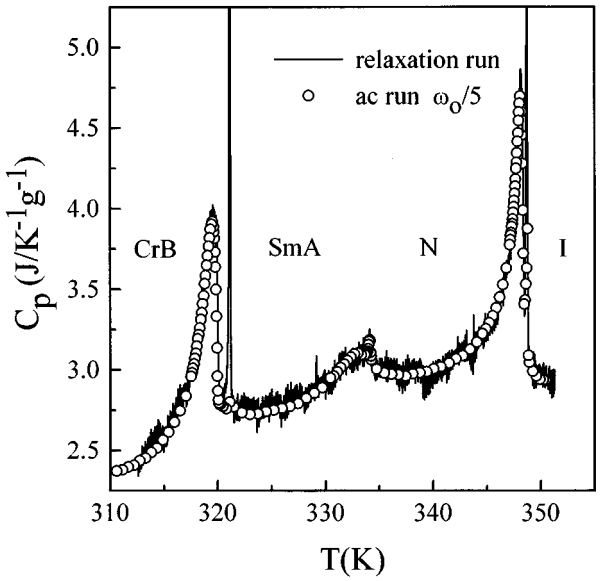

FIG. 1. Heat capacity for 4O.8 in a $\rho = 0.08$ aerogel. The ac calorimeter points correspond to the static specific-heat capacity. The relaxation data agree well with C_p(ac), except for the presence of two sharp spikes in the N-I and Sm-A–Cr-B regions.

$$\Delta C_p = A^{\pm} t^{-\alpha}(1 + D^{\pm} t^{0.5}) + B_c , \tag{5}$$

where $\Delta C_p = C_p - C_p$ (background) and $t = |T - T_c|/T_c$ is the reduced temperature. Fits over the range $t \leq 5.9 \times 10^{-3}$ yielded $\alpha = 0.133$ and $A^-/A^+ = 1.243$, which agree well with the values $\alpha = 0.134 \pm 0.015$ and $A^-/A^+ = 1.132 \pm 0.16$ determined previously [8].

The temperature dependencies of C_p for 4O.8 in aerogels with $\rho = 0.08$ and 0.17 are shown in Figs. 1 and 2. In both cases, data for a relaxation run and low-frequency data from

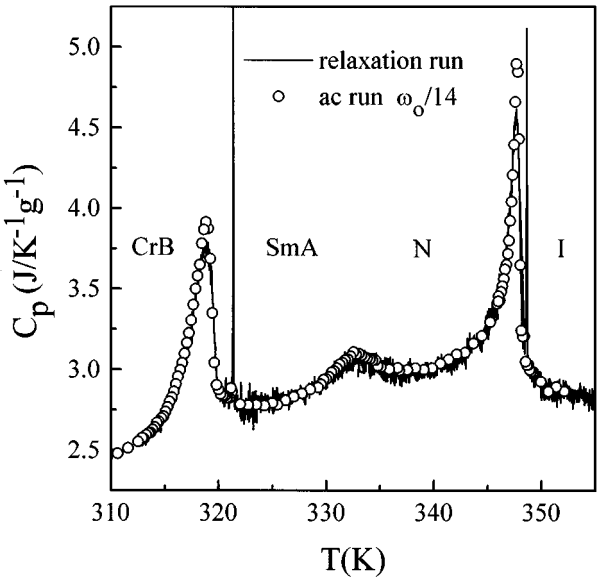

FIG. 2. Heat capacity for 4O.8 in a $\rho = 0.17$ aerogel. The ac calorimeter points are a close approximation of the static specific-heat capacity, except very close to the maxima of the rounded N-I and Sm-A–Cr-B peaks. As in Fig. 1, the relaxation data exhibit two additional sharp spikes.

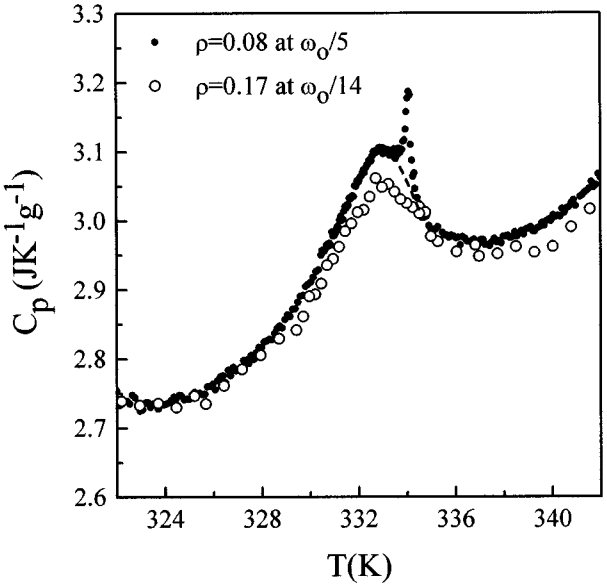

FIG. 3. Detailed view of static C_p data in the vicinity of the $N-$Sm-A transition. The integrated areas δH_{NA} are given in Table I. The δH_{NA} value for the $\rho=0.08$ aerogel sample does not include the sharp ''spike'' above the dashed line. The data for the $\rho=0.17$ sample have been shifted slightly (up by 0.5 K) in temperature in order to superimpose the two $N-$Sm-A aerogel peaks. See the text for comments on the spike.

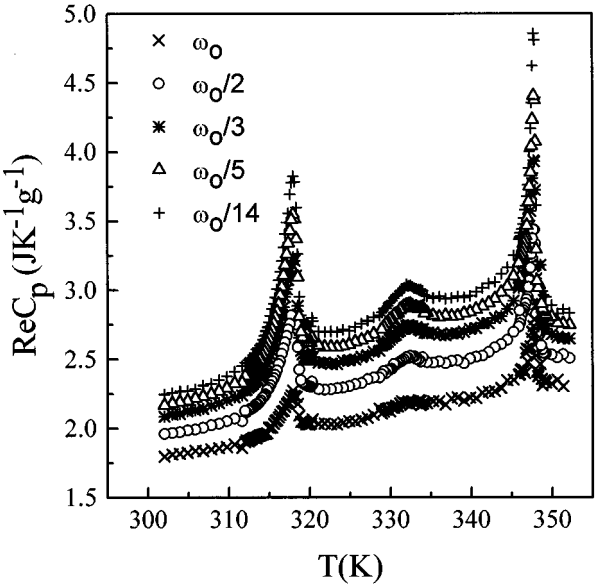

FIG. 4. Temperature dependence of $\mathrm{Re}C_p(\omega,T)$ for 4O.8 in the $\rho=0.17$ aerogel for five typical frequencies in the range $\omega_0/14-\omega_0$, where $\omega_0=0.1963\ \mathrm{s}^{-1}$.

an ac calorimetry run are given. For the $\rho=0.08$ aerogel data in Fig. 1, $C_p(\omega_0/5)$ corresponds to the static heat capacity since $C_p(\omega)$ data from $\omega_0/3$ to $\omega_0/14$ agree well at all temperatures. For the $\rho=0.17$ aerogel data in Fig. 2, $C_p(\omega_0/14)$ is a good approximation to the static heat capacity, except very close to the maxima associated with N-I and Sm-$A-$Cr-B peaks. As will be shown later, there are substantial dynamic effects for 4O.8 in the $\rho=0.17$ aerogel.

The relaxation run data shown in Figs. 1 and 2 agree very well with the C_p(ac) data, except they exhibit extremely sharp effective heat-capacity ''spikes'' on the high-temperature side of the rounded N-I and Sm-$A-$Cr-B peaks. Such features are characteristic of latent heat effects for a strongly first-order transition with a very narrow ($\sim$300 mK here) coexistence range. It is tempting to think of such spikes as arising from a small amount of excess bulk 4O.8, but these spikes are shifted in temperature by a substantial amount relative to the position of the bulk 4O.8 transition temperature, as indicated in Table I. The first-order nature of these relaxation spikes is confirmed by a careful examination of the ac C_p magnitude and the phase shifts between the heat input power and the T_{ac} oscillation, which show small but characteristic anomalies associated with two-phase coexistence at a first-order transition.

There is also a small but sharp extra feature in the relaxation data just above the rounded $N-$Sm-A peak in the $\rho=0.08$ aerogel sample. In this case the C_p(ac) data show a comparable feature, which can be seen in the detailed view of the $N-$Sm-A region given in Fig. 3. The agreement between data obtained with the ac method and the relaxation method indicates that no latent heat is involved here. Thus there is a small second-order $N-$Sm-A extra feature analogous to the first-order N-I and Sm-$A-$Cr-B spike features described above. All of these three small features have bulk-like characteristics in terms of the order of the transitions and their sharpness. There is no comparable extra C_p feature shown in Fig. 3 for the $\rho=0.17$ aerogel sample, but a small anomaly was observed above the rounded $N-$Sm-A aerogel peak for one of the other $\rho=0.17$ aerogel samples that we studied. On this evidence we tentatively conclude that a very small second-order extra feature also occurs above the large rounded $N-$Sm-A peak for these $\rho=0.17$ samples.

The temperature shifts from bulk 4O.8 values for both the large rounded 4O.8-aerogel peaks and the sharp spikes discussed above are given in Table I together with enthalpy values corresponding to the large features. The latent heats associated with the sharp N-I and Sm-$A-$Cr-B relaxation spikes in both aerogels are estimated to be 0.16–0.18 J for N-I and 0.20–0.22 J for Sm-$A-$Cr-B per gram of 4O.8 contained in the aerogel sample, corresponding to roughly 4% of the integrated enthalpy observed in the corresponding large rounded aerogel features.

As shown in Figs. 4 and 5, strong dynamical effects were observed for 4O.8 in the $\rho=0.17$ aerogel. These include both dispersion (frequency dependence) in the real part of C_p and a substantial imaginary C_p component. Although dynamical effects were observed at all temperatures, these effects are most pronounced in the vicinity of the phase transitions. Note that the sharpness of the excess C_p transition peaks increases as the frequency is lowered.

A comparable set of $C_p(\omega)$ measurements was made for 4O.8 in the $\rho=0.08$ aerogel at 12 frequencies over the $\omega_0/14-\omega_0$ range while T was held constant and then stepped through the desired range. In addition, a temperature scan was made at the constant frequency $2\omega_0$. Below $\omega_0/5$, there was no dispersion (i.e., C_p was independent of ω) and no imaginary component. Very weak dynamical effects were observed at higher frequencies, but the characteristic relaxation time must be appreciable shorter than for $\rho=0.17$ samples. The difference $[\mathrm{Re}C_p(\omega_0/5)-\mathrm{Re}C_p(2\omega_0)]$ was

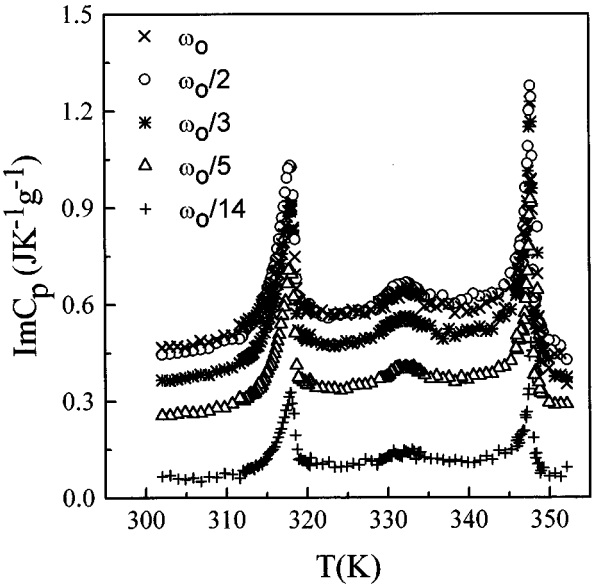

FIG. 5. Temperature dependence of $\mathrm{Im}C_p(\omega,T)$ for 4O.8 in the $\rho=0.17$ aerogel for five typical frequencies.

only -0.07 J K^{-1} g^{-1} ($\sim$3%) for T values far from any transition temperature and -0.5 J K^{-1} g^{-1} ($\sim$15%) for T values corresponding to the positions of the *N*-*I* and Sm-*A*–Cr-*B* peaks. Thus the relaxation of 4O.8 in $\rho=0.08$ aerogels is not well characterized by data in our frequency window and will not be discussed further.

An attractive representation of the dynamical heat capacity data for 4O.8 in the $\rho=0.17$ aerogel is a so-called Cole-Cole plot of $\mathrm{Im}C_p(\omega,T)$ vs $\mathrm{Re}C_p(\omega,T)$ for all available frequencies at a given temperature. Such plots were made and fit with a model to be described below for 137 temperatures over the range 298–352 K. Examples of these Cole-Cole plots at temperatures near the maxima of $\mathrm{Re}C_p$ for *N*-*I*, *N*–Sm-*A*, and Sm-*A*–Cr-*B* transitions are shown in Figs. 6–8.

It is clear from Figs. 6–8 that the relaxation does not have a simple Debye form, which would yield semicircular Cole-Cole plots. The polydispersity is clearly changing with $\Delta T=T-T_{\mathrm{peak}}$ and becoming greater as $\Delta T\rightarrow 0$. This is especially true for the data near the *N*-*I* and Sm-*A*–Cr-*B* peaks. Furthermore, the data indicate an asymmetric distribution of relaxation times with a quite strong tail toward longer relaxation times near the transition temperatures.

A suitable form for representing all the relaxation data for 4O.8 in the $\rho=0.17$ aerogel is the so-called inverse Havriliak-Negami equation [13]

$$C_p^*=C_p(0)-[C_p(0)-C_p(\infty)]\left\{\frac{(i\omega\tau)^{1-\alpha}}{1+(i\omega\tau)^{1-\alpha}}\right\}^{\beta}. \quad (6)$$

This type of form has been used to represent non-Debye behavior in the dielectric constant of certain glasses and polymer systems. Equation (6) is the thermal analog of the original dielectric expression.

The quantity $C_p(0)$ is the static thermodynamic specific-heat capacity, $C_p(\infty)$ is the high-frequency plateau value of C_p with respect to this relaxation process (although it may

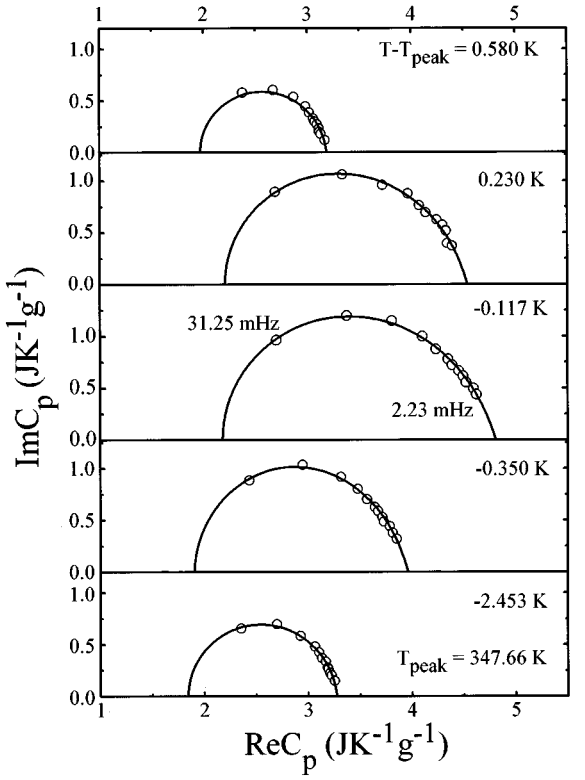

FIG. 6. Cole-Cole plots of $\mathrm{Im}C_p(\omega,T)$ versus $\mathrm{Re}C_p(\omega,T)$ for five temperatures near T_{peak} for the *N*-*I* transition. The curves are fits with the inverse Havriliak-Negami function Eq. (6).

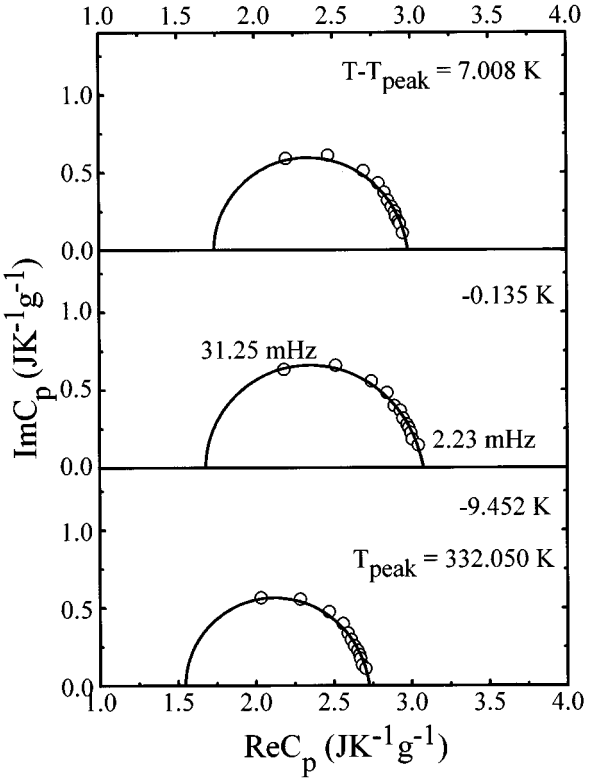

FIG. 7. Cole-Cole plots of $\mathrm{Im}C_p(\omega,T)$ versus $\mathrm{Re}C_p(\omega,T)$ for three temperatures near T_{peak} for the *N*–Sm-*A* transition. The curves are fits with the inverse Havriliak-Negami function Eq. (6).

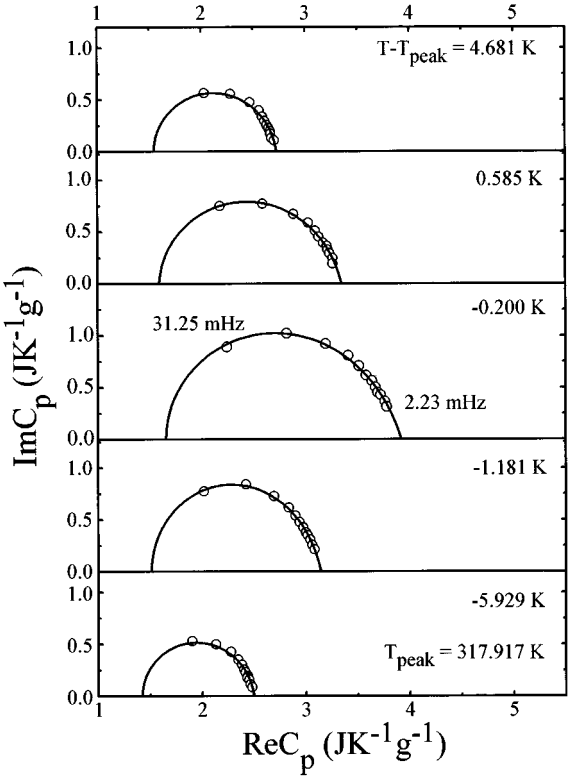

FIG. 8. Cole-Cole plots of Im$C_p(\omega,T)$ versus Re$C_p(\omega,T)$ for five temperatures near T_{peak} for the Sm-A–Cr-B transition. The curves are fits with the inverse Havriliak-Negami function Eq. (6).

not be the true infinite frequency value if some other higher-frequency relaxations play a role), and τ is the relaxation time. Initial fits in which both the parameters α and β were allowed to be free yielded $\alpha = 0 \pm 0.03$, so α was held fixed at zero for all the fits described here. Typical examples of such fits are shown in Figs. 6–8. It is clear that our data are distributed mostly on the low-frequency side of the relaxation. Thus the $C_p(0)$ values are quite well determined, whereas $C_p(\infty)$ values involve a greater extrapolation and are less certain.

The temperature dependencies of the fitting parameter β and the relaxation time τ are given in Figs. 9 and 10. Figure 9 shows a dramatic increase in polydispersity close to the N-I and Sm-A–Cr-B transitions and a milder variation near the N–Sm-A transition. The τ behavior in Fig. 10 is analogous: a very rapid slowing down in the N-I region, a moderate slowing down in the Sm-A–Cr-B region, and a very mild variation near the N–Sm-A transition. The $C_p(0)$ and $C_p(\infty)$ values obtained from fits with Eq. (4) are shown as functions of T in Fig. 11. The $C_p(0)$ values are very close to the $C_p(\omega_0/14)$ experimental values given in Fig. 2, except, of course, $C_p(0)$ is slightly larger in the vicinity of both the N-I and Sm-A–Cr-B peaks.

IV. DISCUSSION

The static thermal properties of 4O.8 in aerogels will be discussed first, beginning with the sharp C_p spike features observed at temperatures slightly above those for the principal large rounded C_p peaks that are associated with transi-

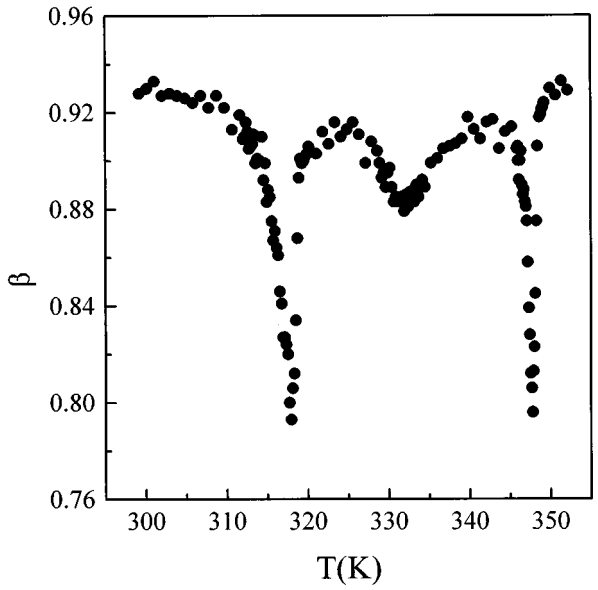

FIG. 9. Temperature variation of the relaxation parameter β in Eq. (6).

tions occurring in the pores of the aerogels. The N-I and Sm-A–Cr-B spikes seen very clearly in relaxation runs correspond to strongly first-order transitions with narrow ($\sim$300 mK) two-phase coexistence regions. The latent heats measured for these two spike regions are small but not negligible. If one assumes that the latent heat per gram for these transitions is comparable to ΔH for bulk 4O.8, roughly 4% of the 4O.8 in the aerogel is needed to account for the magnitude of these two features. The N–Sm-A spike shown as a C_p(ac) feature in Fig. 3 and also seen in relaxation runs on 4O.8 in the $\rho = 0.08$ aerogel is a second-order transition feature.

Somewhat similar N-I and N–Sm-A sharp spikes were observed in ac calorimetry data for 8CB in silica aerogels, but there are significant differences. The spikes seen for

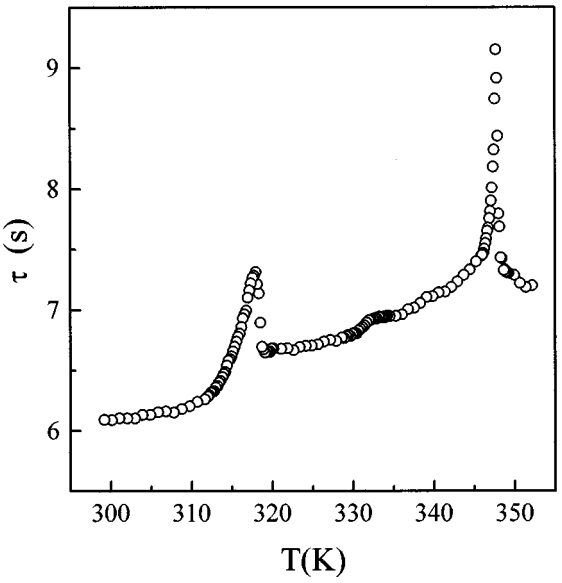

FIG. 10. Temperature dependence of the relaxation time τ for 4O.8 in the $\rho = 0.17$ aerogel.

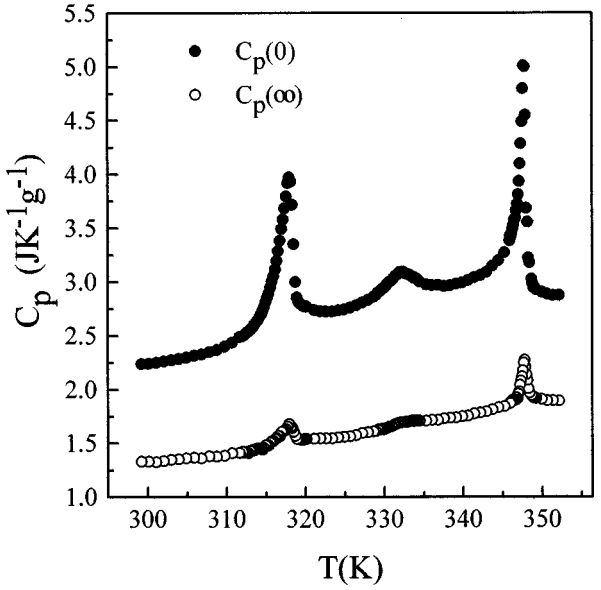

FIG. 11. Temperature variation of $C_p(0)$ and $C_p(\infty)$ resulting from fits to Cole-Cole plots with Eq. (6).

8CB-aerogel samples were assigned to a small surface excess of bulk 8CB since the temperatures of these spikes agreed with the bulk 8CB transition temperatures and the C_p(ac) spikes could be eliminated by surface drying with filter paper [5]. No relaxation calorimetry was done on 8CB-aerogel samples, so the *N-I* latent heat associated with that spike is not known, nor is it known if any relaxation spike persisted after drying the surface. The major difference between these sharp spike features in 4O.8-aerogel and 8CB-aerogel samples is the large shift in temperature between the locations of the aerogel spikes and the corresponding bulk 4O.8 transitions. As shown in Table I, the magnitude of such shifts differed for different transitions but was essentially the same for a given transition in both the $\rho=0.08$ and 0.17 aerogels. The fact that the spikes are sharp indicates that the 4O.8 giving rise to them is in a homogeneous environment, but the T shifts of ~ 1.3–~ 4.5 K shows that this material is substantially perturbed relative to pure bulk 4O.8. The fact that the temperature shifts are negative indicates that silica acts as a disordering surface [14] for 4O.8. We have no way to identify the location of this material, but it seems rather unlikely that it is on the external surface since the samples were surface dried prior to being placed in the silver cell.

We believe that the reason for the large transition temperature shifts observed here is stronger anchoring of 4O.8 on silica than occurs with 8CB. The surface of silica aerogel particles are covered with hydroxyl groups, and thus one must consider possible hydrogen bonding interactions between the surface and the liquid-crystal molecules. 8CB molecules are not able to form hydrogen bonds since the basicity of the nitrogen in the cyano group is very low. However, both the oxygen in the butyloxy group and the nitrogen in the Schiff base linking group between the rings in 4O.8 are basic enough to form hydrogen bonds of moderate strength. In addition, there could be dipolar interactions between the surface and the transverse dipole that exists in 4O.8. Thus there is a competition between liquid-crystal–silica-surface interactions (which hinder ordering) and liquid-crystal–liquid-crystal interactions (which favor ordering). The stronger 4O.8-surface anchoring should shift all transitions to lower temperatures, and one would expect this to be most pronounced for orientational ordering, i.e., the *N-I* transition, as is observed.

Let us now consider the major C_p peaks that arise from the 4O.8 contained in the aerogel ''pores.'' Some aspects of the *N-I* and *N*–Sm-*A* peaks agree with features seen previously in 8CB-aerogel samples [5]. These peaks are broader and more rounded than the comparable peaks in bulk 4O.8 and are shifted down in temperature relative to the sharp C_p spikes. The *N-I* shift T_c(aerogel)-T_c(spike) is -0.5 K for the $\rho=0.08$ aerogel and -0.9 K for the $\rho=0.17$ aerogel. The corresponding *N-I* shifts for 8CB-aerogel samples were -0.45 and -0.72 K. The *N*–Sm-*A* shift is -1.0 K for the $\rho=0.08$ aerogel and approximately -1.7 K for the $\rho=0.17$ aerogel (a value that is somewhat uncertain due to difficulty in precisely locating the *N*–Sm-*A* spike position in this aerogel). The corresponding *N*–Sm-*A* shifts for 8CB-aerogel samples were -0.98 and -1.62 K. It must, of course, be kept in mind that the T_c(spike) values for 8CB agreed with the bulk transition temperatures, whereas those for 4O.8 are substantially shifted from bulk values.

It should be stressed that there is an important difference between the *N-I* peaks for 8CB and 4O.8 in aerogels with density $\rho=0.08$ and 0.17. In both of these aerogels, 8CB continues to exhibit a region of two-phase coexistence (i.e., a weak first-order character) and the 8CB *N-I* transition becomes continuous only in higher-density (lower-porosity) aerogels. In contrast to this, the present 4O.8-aerogel samples show no indications of first-order behavior. The ac phase shifts associated with the large *N-I* peak and also the large Sm-*A*–Cr-*B* peak (a strongly first-order transition in the bulk) give no indications of two-phase coexistence. Nor are there any smeared latent heat effects since ac calorimetry and relaxation calorimetry agree. It is predicted theoretically [15] that a quenched random field can convert first-order into continuous transitions. Thus it appears that the magnitude of such random fields for a given aerogel is greater for 4O.8 than for 8CB, which would be consistent with the idea of stronger anchoring for 4O.8.

Another difference between 4O.8-aerogel samples and 8CB-aerogel samples is the trend in the integrated enthalpies as a function of aerogel density. As shown in Table I for all three transitions (*N-I*, *N*–Sm-*A*, and Sm-*A*–Cr-*B*), δH values for 4O.8 in the $\rho=0.08$ aerogel are $(78.5\pm 1)\%$ of the *total* enthalpies (integrated enthalpy δH plus any latent heat ΔH that may exist) for bulk 4O.8 and the δH values in the $\rho=0.17$ aerogel are $(70.5\pm 1)\%$ of the total bulk enthalpies. In the 8CB-aerogel system, δH_{NI}(aerogel) is a larger percent of the bulk value and δH_{NI}(aerogel) values decreases slower with increasing aerogel density than do δH_{NA}(aerogel) values.

In the more extensive study of 8CB in four aerogels it is concluded that the thermal behavior reflects primarily random-field effects rather than surface effects or finite-size effects. We believe that the dominance of random fields over finite size is still valid for 4O.8 in high-porosity aerogels, but surface effects may play a larger role here due to stronger anchoring and this may help to explain the large temperature shifts for the small but sharp spikes. It would be very attrac-

tive to carry out light-scattering and x-ray studies for 4O.8-aerogel samples like those that have been done on the 8CB-aerogel system [1,9,16,17].

As a final topic, a few remarks will be made about the dynamical aspects of our 4O.8-aerogel data. It is clear from Figs. 4 and 5 that a frequency dependence is observed for $\mathrm{Re}C_p$ in the $\rho=0.17$ aerogel samples over our entire temperature range, but for temperatures away from transition regions $\mathrm{Re}C_p(\omega_0/14)$ is very close to the static specific-heat capacity. Presumably the relaxation behavior away from phase transition temperatures is due to the poor thermal conductivity of liquid crystals embedded in an aerogel structure. There are, however, interesting pseudocritical relaxation effects at the phase transitions that are not seen in the bulk 4O.8 sample. Figures 9 and 10 show that the polydispersity of the relaxation spectrum and the effective relaxation times τ vary strongly near both the N-I and Sm-A–Cr-B transitions and more mildly near the N–Sm-A transition. Again it seems reasonable that strong surface anchoring (or, more generally, strong random-field perturbations) could account for such long relaxation times for 4O.8 when it is an aerogel. Note that random fields are weaker in a $\rho=0.08$ aerogel and the relaxation effects observed for 4O.8 in that aerogel seem to be shifted to higher frequencies.

The behavior of the $C_p(\infty)$ temperature dependence that arises from fits to Cole-Cole plots with Eq. (6) (see Fig. 11) suggests that there may be a second, higher-frequency relaxing contribution to C_p that lies above our frequency window. Such an extra high-frequency contribution has been reported in the case of dynamics near the Sm-C–Sm-I critical point [10]. If a second relaxing contribution did not exist, one would expect $C_p(\infty)$ to correspond to a smooth background heat capacity that was linear in T. However, the speculation must be treated with care since the available data do not approach $C_p(\infty)$ very closely and Eq. (6) is an empirical form that may not provide a reliable extrapolation to much higher frequencies.

ACKNOWLEDGMENTS

The authors wish to thank H. Haga, G. Iannacchione, and O. Lavrentovich for helpful discussions. This work was supported in part by the National Science Foundation under Grant No. DMR 93-11853. Z.K. wishes to acknowledge support from the Fulbright program and the Ministry of Science of Slovenia.

[1] *Liquid Crystals in Complex Geometries Formed by Polymer and Porous Networks*, edited by G. P. Crawford and S. Zumer (Taylor and Francis, London, 1996).
[2] G. S. Iannacchione and D. Finotello, Phys. Rev. Lett. **69**, 2094 (1992); Phys. Rev. E **50**, 4780 (1994).
[3] G. S. Iannacchione, G. P. Crawford, S. Zumer, J. W. Doane, and D. Finotello, Phys. Rev. Lett. **71**, 2595 (1993); Phys. Rev. E **53**, 2402 (1996).
[4] S. Qian, G. S. Iannacchione, and D. Finotello, Phys. Rev. E **53**, R4291 (1996).
[5] L. Wu, B. Zhou, C. W. Garland, T. Bellini, and D. W. Schaefer, Phys. Rev. E **51**, 2157 (1995), and references cited therein.
[6] B. Zhou, G. S. Iannacchione, and C. W. Garland, Liq. Cryst. (to be published).
[7] K. J. Lushington, G. B. Kasting, and C. W. Garland, J. Phys. Lett. (Paris) **41**, L419 (1980).
[8] K. J. Stine and C. W. Garland, Phys. Rev. A **39**, 3148 (1989).
[9] T. Bellini, N. A. Clark, C. D. Muzny, L. Wu, C. W. Garland, D. W. Schaefer, and B. J. Oliver, Phys. Rev. Lett. **69**, 788 (1992).
[10] H. Yao, T. Chan, and C. W. Garland, Phys. Rev. E **51**, 4585 (1995), and references cited therein.
[11] Y. H. Jeong, G. Nounesis, C. W. Garland, and R. Shashidhar, Phys. Rev. A **40**, 4022 (1989).
[12] X. Wen, C. W. Garland, and M. D. Wand, Phys. Rev. A **42**, 6087 (1990).
[13] C. J. F. Böttcher and P. Bordewijk, *Theory of Electric Polarization* (Elsevier, Amsterdam, 1978), p. 75.
[14] H. Yokoyama, J. Chem. Soc. Faraday Trans. II **84**, 1023 (1988).
[15] A. Falicov and A. N. Berker, Phys. Rev. Lett. **76**, 4380 (1996), and references cited therein.
[16] X.-I. Wu, W. I. Goldburg, M. X. Liu, and J. Z. Xue, Phys. Rev. Lett. **69**, 470 (1992); T. Bellini, N. A. Clark, and D. W. Schaefer, *ibid.* **74**, 2740 (1995).
[17] N. A. Clark, T. Bellini, R. M. Malzbender, B. N. Thomas, A. G. Rappaport, C. D. Muzny, D. W. Schaefer, and L. Hrubesh, Phys. Rev. Lett. **71**, 3505 (1993).